Multi-Scale Characterization of Asphalt Mortar with Indentation Test

Hassan Fadil[1], Denis Jelagin[2], Per-Lennart Larsson[3], Manfred N. Partl[4]
（[1] KTH – Royal Institute of Technology, Sweden, hassanf@kth.se）
（[2] KTH – Royal Institute of Technology, Sweden, denis.jelagin@abe.kth.se）
（[3] KTH – Royal Institute of Technology, Sweden, plla@kth.se）
（[4] Empa, Swiss Federal Laboratories for Materials Science and Technology, Switzerland, manfred.partl@empa.ch）

ABSTRACT

Reliable determination of material properties is a key component for modeling and understanding performance of asphalt pavements. This paper deals with the potential use of instrumented indentation tests for viscoelastic characterization of asphalt mortar as a new alternative to existing techniques. The main focus lies on the potential of indentation tests for multi-scale measurement of shear relaxation modulus. A three-dimensional finite element model of a rigid spherical indenter penetrating an asphalt mortar sample is developed and used to model indentation tests performed at different material scales. The asphalt mortar is modeled as an idealized fine aggregate composite with elastic spheres, suspended within a viscoelastic bitumen mastic matrix. Based on the obtained numerical results the scale-dependency of the shear relaxation modulus measured with the indentation test is investigated. The minimum indentation radius required for obtaining representative properties, measured at the mortar scale, is determined. The viscoelastic parameters obtained from the indentation model are compared to those obtained using a representative volume element (RVE) for the asphalt mortar. Periodic boundary conditions for the homogenization are utilized. Moreover, the effect of indentation depth at the same contact area is investigated, finding that the contact depth has a minimal effect. In this way, the paper provides a new impulse for linking the mortar and asphalt scales in the multiscale modeling of asphalt mixtures.

Keywords: Indentation, Asphalt mortar, Asphalt, Multiscale, Viscoelasticity, FEM.

1. INTRODUCTION

Instrumented indentation tests have been used to measure the viscoelastic and adhesive properties of asphalt binders at micro- as well as macro-scales cf. [1]–[4]. As compared to the conventional rheological characterization methods for bituminous materials (i.e. bitumen, bitumen-filler mastics and bitumen- fine sand asphalt mortar), indentation tests have the advantage of being able to probe the local properties of materials, thus allowing to measure the linear viscoelastic properties across different structural size scales. Accordingly, the same testing technique may be applied for both probing individual phase properties in bitumen-aggregate composites and measuring the composite properties at size scales relevant for the mechanical behavior and aging processes as well as various asphalt damage mechanisms, such as fatigue, rutting and moisture damage, cf. [5], [6].

In a recent study by Fadil et al. [7] a new methodology for viscoelastic characterization of bituminous material with spherical indentation test has been proposed, which allows extracting the linear viscoelastic properties of materials at arbitrary non-decreasing loading. The method

developed in [7] has been applied to measure viscoelastic properties of bitumen and bitumen-filler mastics. The intention of the present study is to extend the methodology developed in [7] to the multi-scale characterization of bituminous materials.

Consequently, this paper aims to investigate numerically the effect of the indenter size on the measured apparent shear relaxation modulus of a bitumen-aggregate composite. The focus is on the viscoelastic characterization of asphalt mortar, i.e. a mixture of bitumen with the aggregates smaller than 2.36 mm. In order to determine macro-scale viscoelastic properties of mortar, a finite element model (FE) is developed with a representative volume element (RVE) for mortars, where the aggregate phase is represented with randomly distributed elastic spheres in a viscoelastic matrix. Multi-scale modelling is applied for improving computational efficiency. The influence of the indentation test parameters on the measured viscoelastic properties of mortar is investigated with the FE model for spherical indentation on inhomogeneous specimens. The shear relaxation functions, $G(t)$, from the indentation tests are compared then with those from RVE modelling. It is shown that the measurement scale can be controlled efficiently by performing indentation tests with different indenter-specimen contact areas. Based on the numerical results, the indentation test parameters for the macro-scale characterization of asphalt mortar as well as its individual components are identified.

2. COMPUTATIONAL STUDY

The micro-mechanical FEM model for asphalt mortar is used for two types of numerical analysis. First, in order to identify homogenized viscoelastic properties of asphalts mortar, a strain controlled periodic boundary conditions (PBC) are specified for a material's RVE, the PBC is utilized to reduce the size of the model. Secondly, a model of instrumented indentation test on asphalt mortar is set up and the analysis procedure proposed in [7] is used to obtain the apparent material properties from the analysis results.

The mortar is modelled in the present study as a composite material consisting of elastic aggregates in a size range 0.3 to 2.36 mm, embedded into viscoelastic bitumen-filler mastics. The aggregates concentration in mortar is assumed to be 33% by volume, corresponding to the porous asphalt mortar [8]. The assumed size distribution of the aggregates is reported in Table 1.

TABLE 1 The assumed aggregate size distribution

Sieve size (mm)	0.075	0.15	0.3	0.6	1.18	2.36
Passing percentage (by volume)	5.2	8.1	12.3	17.9	28.6	39.1

The model uses two separate size scales, in order to improve computational efficiency. In particular, aggregates smaller than 0.6 mm are relegated to the smaller scale, here denoted sub-mortar, where the material is assumed to be comprised of bitumen based mastic, as a matrix, and randomly distributed spherical aggregates. The mortar scale model is in turn composed of randomly distributed spherical aggregates in the range between 0.6 mm to 2.36 mm, embedded in a viscoelastic matrix with properties as obtained for the homogenized viscoelastic sub-mortar scale. These scales are illustrated in Figure 1 (a). This aggregate size range attributed to the mortar scale follows the definition in [9]. Figure 1 (b), shows a representation of the models with spherical aggregates randomly distributed within a viscoelastic matrix.

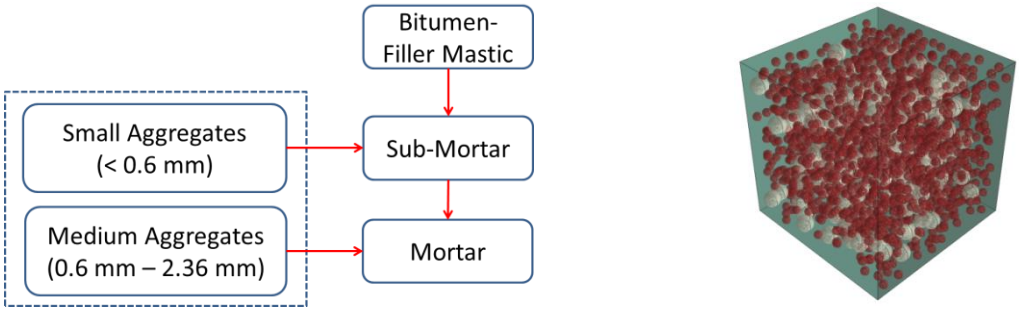

FIGURE 1 (a) A schematic illustrating the different scales and their constituents (b) mortar model showing the aggregates idealized as spheres

The 33% aggregate concentration of the mortar phase is distributed between the two scales, sub-mortar and mortar, according to the aggregate size distribution shown in Table 1; correspondingly the sub-mortar model has an aggregate volume percentage of 15% and mortar model has an aggregate volume percentage of 18%.

Mortar and mastic are both assumed to be incompressible with constant Poisson's ratio. Aggregates are assumed to be linear elastic, with Young's modulus, $E = 39.3$ GPa and Poisson's ratio $v = 0.23$, corresponding to elastic parameters of limestone [10]. The aggregates are idealized as spheres to simplify the modelling.

The matrix at the sub-mortar model is assumed to be comprised of bitumen-filler mastics, with its $G(t)$ obtained as a power law fit of the measured shear relaxation modulus of bitumen mixed with 20% by volume of hydrated lime filler at $T = 0°C$ reported in [7].The spherical aggregates are randomly distributed within the matrix as follows: 80 spheres of 0.6 mm diameter and 1747 spheres of 0.3 mm diameter.

The mortar phase is assumed to be comprised of a matrix with the $G(t)$ obtained as the homogenized shear relaxation modulus of the sub-mortar. The homogenized sub-mortar $G(t)$ is obtained using periodic boundary conditions model as described below. The spherical aggregates are randomly dispersed within the matrix and are represented by 1489 and 148 spheres of 1.18 mm and 2.36 mm diameters respectively.

The finite element meshes used in the present study is shown in Figure 2 (a,b) for the RVE and the indentation test analysis respectively. As seen in Figure 2 (a), the RVE model has a cubical form with a side length 10 times the size of the largest aggregate, i.e. $L = 23.6$ mm. The periodic boundary conditions are applied, where strain constraint equations are enforced on the facial nodes of the mesh in order to simulate the deformation of a RVE as part of an infinite medium [11]. The ABAQUS plugin HOMTOOLS [12] was used to automate the generation of the equations, coupling the displacement of the nodes on opposing faces of the RVE cube.

To simulate a Heaviside function loading, the RVE is loaded with a prescribed, uniform effective strain $\epsilon_z = 2\%$, in a static analysis and the strain for viscoelastic analysis is maintained during 10 seconds. The effective values of the resulting stresses are recorded in the three Cartesian directions x, y and z, namely σ_x, σ_y and σ_z respectively. The 3D Hooke's law, in conjuction with the viscoelastic correspondence principle, is utilized to calculate the apparent shear relaxation function, $G(t)$, for the material. The PBC is used to obtain the homogenized $G(t)$ of sub-mortar and mortar models.

The influence of indentation radius on the measured $G(t)$, is investigated with the FE model depicted in Figure 2 (b). A sketch of the indentation test is shown in Figure 2 (c), along with the

relevant geometric parameters; where R is the curvature radius of the indenter, h is the indentation depth, a is the contact area radius and P is the indentation load. The FE model is composed of two segments, the cubic model of mortar material with a side $L = 23.6$ mm modelled with the micromechanical approach outlined above and a volume surrounding the indentation model is used to extend the model to $L = 236$ mm for mitigating the edge effects as described in [7]. In order to facilitate computations, this surrounding material is modelled as homogeneous viscoelastic material with properties obtained from the mortar RVE model above.

An indentation relaxation test, i.e. $h(t) = h_o \times H(t)$, where h_o is a prescribed indentation depth and $H(t)$ is the Heaviside step function, is modelled for the duration of 10 seconds. The $P(t)$ history obtained numerically is used in the Eq.(1) to calculate the corresponding shear relaxation function, $G(t)$, cf. [7]:

$$G(t) = \frac{3}{8}\frac{P(t)(1-\nu) \times R}{a^3} \tag{1}$$

where a is obtained by Eq.(2):

$$a = \sqrt{R \times h_o} \tag{2}$$

As discussed in e.g. [13], the scale of the stress field induced in the linear elastic or viscoelastic specimen during the spherical indentation is controlled by the radius of the contact area, a. In the experiment, the size of the contact area can be controlled by either changing, the indenter curvature radius R or the indentation depth h. Presently, the indenter curvature radii are varied which results in contact area sizes a in a range of 0.45-18.0 mm. Furthermore, in order to evaluate the influence of the indentation depth h on the measurements, comparative simulations are performed for indentations with the same indentation areas but different indentation depths. Two sets of simulations are performed with the same indentation area; in the first set, the indenters with the curvature radii $R = 8$ and 200 mm are indented to $h = 0.1$ mm and 0.004 mm respectively. In the second set the curvature radii $R = 3200$ and 800 mm indented to $h = 0.1$ mm and 0.4 mm respectively.

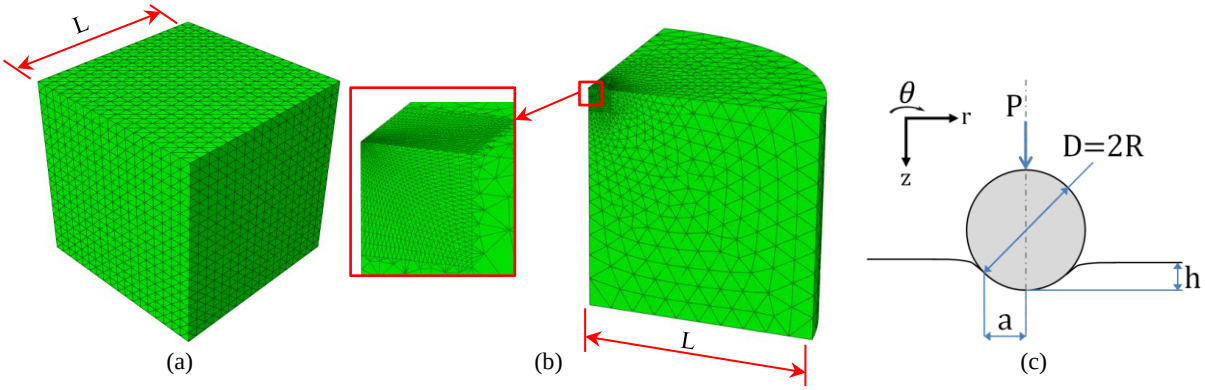

FIGURE 2 (a) indentation model with a zoomed in indentation area mesh, (b) periodic boundary conditions mesh, (c) schematic of indentation with relevant parameters

3. RESULTS AND DISCUSSION

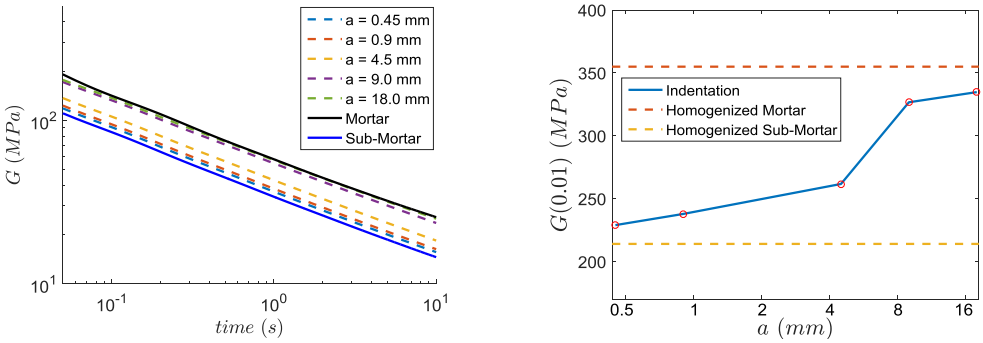

(a) (b)

FIGURE 3 (a) $G(t)$ obtained using indentation, with various radii, compared to the homogenized mortar and sub-mortar $G(t)$, (b) $G(0.01\ s)$ as a function of contact area radius

The $G(t)$ results obtained for each indentation radius are shown in Figure 3 (a) together with the homogenized $G(t)$ for the sub-mortar and mortar models. From the graph it can be concluded that in the indentation tests, the measurements correspond to the effective viscoelastic properties of sub-mortar matrix and homogenized mortar properties can be obtained depending on the dependeing on the contact radii during the test. In particular, at smaller $a = 0.45\ mm$ obtained $G(t)$ is close to the homogenized sub-mortar $G(t)$, with the average difference between indentation test and the homogenized cases being below 8% for the measurement period. At larger values of a, especially at 9 mm and 18 mm, the obtained $G(t)$ is very close to the homogenized mortar properties. The average difference between the homogenized $G(t)$ and the ones obtained with indentation at at $a = 9\ mm$ and $a = 18\ mm$ is 6.5% and 1.4% respectively. Figure 3 (b), depicts the change in the obtained $G(0.01\ s)$ for different values of a. It also shows that the measured $G(t)$ approaches both the sub-mortar and mortar homogenized properties asymptotically for small and large values of a respectively. Due to the simplification of the model, the aggregate size chosen to distinguish the sub-mortar from mortar, in this case 0.6 mm, determines the $G(t)$ obtained at small values of a, however, its effect on the obtained $G(t)$ of mortar needs further investigation.

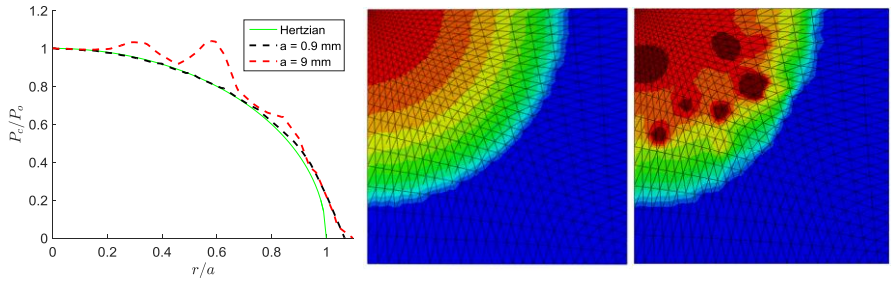

(a) (b) (c)

FIGURE 4 pressure distribution under the indenter, (a) contact pressure P_c normalized with the contact pressure at the center P_o vs. distance from center of contact r normalized with the indentation radius a, (b) pressure distribution for 0.9 mm indentation radius, (c) pressure distribution for 9 mm indentation radius

Figure 4 (a), shows the normalized distribution of the contact pressure along a line from the center of indentation to the boundary of the contact area is presented for $a = 0.9\ mm$ and $a = 9\ mm$ and compared to the Hertzian contact pressure. It can be seen clearly that the small $a = 0.9\ mm$, the contact pressure distribution shape is similar to the Hertzian contact, which

explains the fact that the measured properties are closed to the homogenized sub-mortar matrix. However, for large $a = 9\,mm$, the contact pressure distribution does not match the Hertzian shape, showing a number of spikes. This is illustrated further in Figures 4 (b,c) where the contact pressure distribution over the contact area is presented for $a = 0.9\,mm$ and $a = 9\,mm$. According to Figure 4 (b), the contact pressure distribution for the 0.9 mm indendation radius is smooth whereas for 9mm indendation radius pressure concentrations occur, see Figure 4 (c). This explains the observed spikes in Figure 4 (a) for the 9 mm contact pressure curve, since the indenter interacts with more aggregates near the surface.

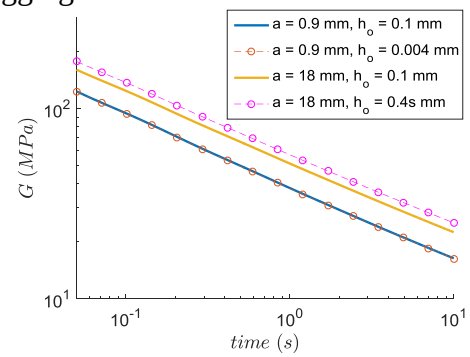

FIGURE 5 $G(t)$ for indentations with similar indentation areas but two different depths

In Figure 5, the influence of the indentation depth on the measurements is examined for the cases of $a = 9\,mm$ and $18\,mm$, i.e. measurments on the sub-mortar and on mortar scale. The results in Figure 5 are shown for the following simulation cases; one case with $a = 0.9\,mm$ and $h_o = 0.1$ mm and $h_o = 0.004$ mm; the other case with $a = 18\,mm$, $h_o = 0.1$ mm and $h_o = 0.4$ mm. As seen in Figure 5, provided that the contact radius does not change the influence of the indentation depth on the measurements is quite small – less than 1% and 12% for the cases of a=0.9 and 18 mm respectively. The higher effect of indentation depth observed for the case of $a = 18\,mm$ as compared to the case of $a = 9\,mm$ can be attributed to the fact that at larger a, more aggregates are interacting with the indenter and accordingly increasing h_o will result in formation of more aggregate-to-aggregate load transferring chains in the material..

4. CONCLUSIONS

From the results presented, it's clear that the indentation test can capture the multiscale properties of asphalt mortars. The indentation scale, as represented by the contact area radius a, has a profound effect on the measured shear relaxation modulus $G(t)$: the smaller the indentation area, the closer is the measured $G(t)$ to the corresponding value for the sub-mortar phase (aggregates 0.6 mm and smaller). Increasing the indentation radius a increases the value of $G(t)$ as it approaches the homogenized $G(t)$ of the mortar phase (aggregates between 0.6 mm and 2.36 mm) obtained using the PBC on the RVE, which acts as an asymptote for the results.

The smallest radius to obtain representative mortar properties was about 8 mm, i.e. about 2.4 times the diameter of the largest aggregate. This resulted in an average measurement difference below 10% as compared to the homogeneous mortar.

The contact pressure distribution deviates from the Hertzian distribution due to the presence of aggregates, especially for larger values of a. As a increases, the indentation test interacts with more aggregates resulting in increase in measured $G(t)$.

Based on the performed simulations, the influence of indentation depth on the test measurements is small as long as the contact area remains the same.

5. REFERENCES

[1] A. Zofka and D. Nener-Plante, "Determination of Asphalt Binder Creep Compliance Using Depth-Sensing Indentation," *Exp. Mech.*, vol. 51, no. 8, pp. 1365–1377, 2011.

[2] D. Jelagin and P.-L. Larsson, "Measurement of the Viscoelastic Properties of Bitumen Using Instrumented Spherical Indentation," *Exp. Mech.*, vol. 53, no. 7, pp. 1233–1244, 2013.

[3] A. Jäger, R. Lackner, and J. Eberhardsteiner, "Identification of viscoelastic properties by means of nanoindentation taking the real tip geometry into account," *Meccanica*, vol. 42, no. 3, pp. 293–306, 2007.

[4] Y. Veytskin, C. Bobko, and C. Castorena, "Nanoindentation investigation of asphalt binder and mastic viscoelasticity," *Int. J. Pavement Eng.*, vol. 17, no. 4, pp. 363–376, 2014.

[5] R. A. Tarefder and A. Zaman, "Characterization of Asphalt Materials for Moisture Damage Using Atomic Force Microscopy and Nanoindentation," *Nanotechnol. Civ. Infrastruct.*, pp. 237–256, 2011.

[6] R. Tarefder and H. Faisal, "Nanoindentation Characterization of Asphalt Concrete Aging," *J. Nanomechanics Micromechanics*, vol. 4, no. 1, p. A4013003, 2014.

[7] H. Fadil, D. Jelagin, and P.-L. Larsson, "On the measurement of two independent viscoelastic functions with instrumented indentation tests," *Exp. Mech.*, 2017.

[8] Y. Zhang and Z. Leng, "Quantification of bituminous mortar §ageing and its application in ravelling evaluation of porous asphalt wearing courses," *Mater. Des.*, vol. 119, pp. 1–11, 2017.

[9] Asphalt Institute, *HMA Construction, Manual Series No. 22 (MS-22)*. Lexington, KY: Asphalt Institute, 2001.

[10] L. Wang, *Mechanics of Asphalt: Microstructure and Micromechanics: Microstructure and Micromechanics*. McGraw-Hill Education, 2010.

[11] W. Wu and J. Owino, "Applying Periodic Boundary Conditions in Finite Element Analysis," *Simulia Community Conf.*, no. Figure 1, pp. 707–719, 2014.

[12] S. Lejeunes and S. Bourgeois, "Une Toolbox Abaqus pour le calcul de propriétés effectives de milieux hétérogènes," in *10ème colloque national en calcul des structures*, 2011, pp. 1–9.

[13] K. L. Johnson, *Contact Mechanics*. Cambridge University Press, 1985.